MODELLING FLUID FLOW THROUGH FRACTURED ROCK: EXAMPLES USING TVZ GEOTHERMAL RESERVOIRS

W.M.Kissling[1], S.E.Ellis[1], D. McNamara[1] and C. Massiot[2]

[1]GNS Science, P.O. Box 30386, Lower Hutt, New Zealand

[2] SGEES, Victoria University of Wellington, P.O. Box 600, Wellington, New Zealand

w.kissling@gns.cri.nz

Keywords: *fractures, TVZ, geothermal reservoirs, permeability, fluid flow models, thermo-mechanical models*

ABSTRACT

Geothermal resources are often hosted within volcanic, plutonic, and basement-type lithologies. As such their matrix permeability can be very low and the transport and circulation of geothermal fluids will be dominated by fractures. Understanding the flow of hydrothermal fluid through fractured rock is thus essential to the efficient utilisation of New Zealand's deeper geothermal resources which are hosted in greywacke basement and lavas. In this study we investigate the nature of fluid flow for a variety of simple, single- and multiple-fracture arrangements and widths within Taupo Volcanic Zone (TVZ) greywacke basement and andesite hosted reservoirs, making use of known permeabilities. We present preliminary numerical models of fluid flow through a metre-scale sample of rock for a variety of simple fracture networks, with emphasis on the perturbation of the total flow across the sample with respect to that of a non-fractured sample. Later work will focus on the changes in fracture properties that influence the flow through these samples due to far field stresses and varying mechanical behaviour of the reservoir rock and its fractures, and upscaling these results from metre-scale experiments to kilometre-scale reservoirs. Future research will also test the effect on fluid flow of known fracture spacing and width distributions of TVZ geothermal reservoirs.

1. INTRODUCTION

Structures such as faults and fractures strongly influence the transport and circulation of hydrothermal fluids in geothermal systems, in particular those systems hosted in volcanic, plutonic, and basement lithologies (Brace, 1980; Davatzes and Hickman, 2010a). As such, successful and optimal development of these geothermal fields requires knowledge of the structural character of the reservoir (fracture and fault orientations, widths, lengths, densities, connectivity, fault rock lithology), how these structures relate to the *in-situ* stress field, and what effect variation of these properties have on reservoir fluid flow (Baghbanan and Jing, 2008; Barton et al., 2013).

It is frequently observed that wider fractures and higher fracture densities often occur within permeable zones in geothermal wells (Sheridan and Hickman, 2004; McLean and McNamara, 2011), and that increased fracture connectivity (usually associated with higher fracture lengths) allows increased reservoir fluid flow (Wallis et al., 2012; Barton et al., 2013; Philipp et al., 2013). Additionally, structures preferably aligned within the *in-situ* stress field undergo more frequent crack-seal events thus are more likely to be open to fluid flow (Ito and Zoback, 2000; Sausse et al., 2006; Davatzes and Hickman, 2010b), though this is not necessarily always the case (Laubach et al., 2004).

The main question we wish to address here is how do the properties of fractures (widths, spacings, permeabilities, orientations, etc.) and the *in-situ* stresses within a geothermal system contribute to the bulk permeability of the reservoir rock?

In section 2 of this paper we summarise the known characteristics of faults and fracturing drawn from studies of the TVZ and the geothermal fields it contains, in particular the Rotokawa Geothermal Field. This provides a context for later sections where we demonstrate some basic fluid flow and rock-mechanical modelling of fractured metre-scale rock samples. The emphasis of the flow modelling (section 3) will be on how differing fracture geometries affect the bulk permeability of the rock sample and how these results might be applicable at the reservoir scale. For the rock-mechanical modelling (section 4) the focus is to demonstrate how a simple applied stress field can affect a two-fracture system and modify its flow regime.

2. GEOLOGICAL CONTEXT

The majority of New Zealand's geothermal resources reside within the Taupo Volcanic Zone (TVZ). The TVZ is an extensional, intra-arc basin formed as a result of subduction of the Pacific Plate beneath the North Island of New Zealand (Wilson and Rowland, 2015). NW-SE extension within the TVZ is accommodated by the Taupo Rift, a series of dominantly NE-SW striking normal faults (Nicol et al., 2006). A fair number of the geothermal resources in the TVZ are hosted in reservoir rocks that have a low matrix permeability, such as greywacke basement rock at the Kawerau and Ohaaki Geothermal Fields (Milicich et al., 2015; McNamara et al., 2014; Wood et al., 2001), or andesite lavas such as the Rotokawa Andesite in the Rotokawa Geothermal Field (McNamara et al., 2015; Siratovich et al., 2014). In these reservoirs faults and fractures control fluid flow.

Within the TVZ fractures and faults have been observed at all scales; from regional mapping (Litchfield et al., 2014), 3D modelling of faulting within geothermal fields based on well geology (e.g. Milicich et al., 2014, Wallis et al., 2013), direct measurement of sub-surface fracture properties from borehole image logging (McNamara et al., 2014; Wallis et al., 2012; McLean and McNamara, 2012), observations of structures from drill-core (Massiot et al., 2015), and observations of micro-fracturing from thin sections of drill-core (Siratovitch et al., 2014).

The Rotokawa Geothermal Field is located c.14 km north of Taupo, on the eastern side of the TVZ. The main 320°C reservoir is hosted in the Rotokawa Andesite, an 800-2100 m thick unit of andesite lavas and breccias, overlying greywacke basement. Three large, steeply dipping normal faults show NE-SW strike orientations consistent with the structural fabric of the TVZ (Wallis et al., 2013). Through investigations of microseismicity, fluid chemistry, and tracer tests these faults have been shown to act as barriers to cross-fault fluid flow while allowing fluid flow along the fault plane (along strike and along dip) (Sherburn et al., 2015).

Analysis of acoustic borehole televiewer (BHTV) logs revealed fractures in the Rotokawa Andesite have a dominant NE-SW strike, with some heterogeneity in fracture dip direction, and subordinate fracture sets striking N-S and NW-SE (McNamara et al., 2014, Massiot et al., 2015). Using BHTV logs and drill-core measurement, fractures widths range between 0.5-5 mm (drill-core), and 5-50 mm (BHTV) (Massiot et al., 2015). BHTV logs also revealed that perturbations in the dominant NE–SW (035°/215°) oriented S_{Hmax} direction were the result of slip activity on fractures and faults in the field. Analysis of fractures located within permeable zones in wells revealed a dominant NE-SW strike orientation, and that nearly all permeable zones contained wide fractures and intervals of high fracture density (McNamara et al., 2014). However fractures with similar properties exist outside of these feed zones implying that other structural properties must play a role in this reservoir's structural fluid flow control (e.g. connectivity, fracture length, and fracture fill).

At the microscopic scale Siratovich et al., (2014) found that the Rotokawa andesite is pervasively, isotropically micro-fractured and that the greater the extent of micro-fracturing in the andesite the higher its measured porosity. It is also inferred that the greater the extent of micro-fracturing the higher the Rotokawa Andesite's permeability. This type of structural permeability, while considered to be less critical to the reservoirs fluid flow than macro-scale structures, is important for the overall fluid flow and storage capacity of this reservoir rock.

3. FLOW MODELLING

Much of the previous work on modelling fluid flow in fracture networks has taken place in the context of EGS systems (see section 3.1 for some examples) and is only partially relevant to New Zealand geothermal systems. To this end, in this paper we begin a new 'bottom up' approach to modelling fracture systems. We begin here with a number of simple fracture systems and (in future work) as understanding of these systems improves, complexity will be added until some connection can be made to the fracture networks in an actual TVZ geothermal system. This latter step will involve developing a new thermo-hydro-mechanical modelling code and using it on models of fracture systems which are statistically informed by data from TVZ geothermal fields.

At this stage however, flow modelling will be used to address two different but related questions:

- What is the effective (or bulk) permeability of a metre-scale rock sample with a number of simple fracture configurations?
- How does this bulk permeability scale to reservoir (~kilometre) length scales?

To address these questions a model of a metre-scale sample of fractured rock has been created, as will be described in sections 3.2 - 3.4.

3.1 Previous flow modelling in fracture networks

Much of the previous work on flow modelling in reservoir scale fracture networks has been in the context of EGS or low temperature geothermal systems (see Sausse et al., 2010, Maffucci et al., 2013, Barton et al., 2013, Marakchi et al., 2015), and has been based on simulations using discrete fracture networks (DFN).

The EGS/DFN modelling has highlighted concepts which are likely to be relevant to TVZ systems. One example is the importance of fracture width and spacing distributions on the degree of thermal breakthrough in an EGS reservoir (Doe et al., 2014). In another example, Huang et al. (2013), shows that higher thermal cooling loads produce more complex crack growth patterns which may have some bearing on interpretation of cool reinjection into deep hot TVZ reservoirs.

3.2 Flow simulation code

For the flow calculations presented in this paper we use the code 'tgns' (Kissling, 2014), which is a GNS in-house flow modelling simulation code. This solves the mass and energy conservation equations for the flow of water and heat through a porous medium, supplemented with an up to date description (e.g. Wagner et al., 2000) of the thermo-physical properties of water (density, enthalpy and dynamic viscosity) which appear in these equations. The solution algorithm used in tgns is very similar to that in TOUGH2 (Pruess, 1990), but extra flexibility comes from the ability to include spatial or temporal dependencies in rock properties, boundary conditions and other aspects of model setup which are difficult to do within the TOUGH2 environment.

For the present work tgns is used with computational meshes which are refined in the vicinity of (and within) the fracture(s). Generally, in the areas of highest refinement, the model elements are typically ~10 times smaller than those near the model boundaries. This allows adequate resolution of flow within the fractures themselves and of the perturbations to the flows in the areas where they are largest - at the fracture tips. To generate these meshes the Voronoi mesh generator AMESH (Haukwa, 1998) is used.

3.3 Model setup

In this section we describe a model of a 2-dimensional rock sample 1 m × 1 m which contains (in different models) a variety of simple fracture networks. (Referring to Figure 1), fixed pressure conditions are prescribed on the upper and lower boundaries of 100 and 101 bar respectively, and no flow is permitted across the left and right boundaries. The initial temperature is set to 250°C everywhere in the model domain and the initial conditions for all models are generated by running the homogeneous model (without fractures) until steady conditions and flows are obtained.

The initial state of the model is characterised by a small range of pressure variation and an almost constant temperature. These conditions arise partly because of the choice of boundary conditions, and partly because of the small size of the model domain. The thermo-physical properties of the fluid (liquid in this case) are thus restricted to be almost constant throughout the model. An important consequence of this is that variations of fluid properties are small and are therefore not relevant to the interpretation of results from our numerical flow experiments. For reference, the density, enthalpy and dynamic viscosity of liquid water at the conditions in these experiments (100 bar/250°C) are 806.1 kg/m^3, 1086.4 kJ/kg and 107.5 μPa.s respectively.

In all models, the low-permeability matrix material has material/flow properties of Rotokawa Andesite taken from Sirotavich et al., (2014). In particular, we use a matrix permeability (κ) of 4×10^{-17} m^2, with higher fracture permeabilities ($\kappa \leq 10^{-12}$ m^2). With this matrix permeability the mass flow through the unfractured sample is, using Darcy's law, 2.999×10^{-5} kg/s. This will be our point of comparison for all of the examples which follow.

3.4 Models and Results

3.4.1 Parallel full length fractures

The simplest model of a fracture network is a single fracture, aligned parallel to the direction of flow, which spans the model domain from lower to upper boundary (Figure 1). Here, the model domain is the same as described in section 3.3, but with the addition of a 1cm wide fracture (1% of the model domain). This system has been modelled with fracture permeabilities ranging from 10^{-12} m^2 down to the matrix permeability of 4×10^{-17} m^2.

Because the fracture spans the complete domain, and its permeability is high relative to the matrix, the pressure drop along the fracture is small. This can be seen on Figure 1 where the fracture lies entirely within the innermost green region where (absolute) pressure changes are less than 0.0005 bar.

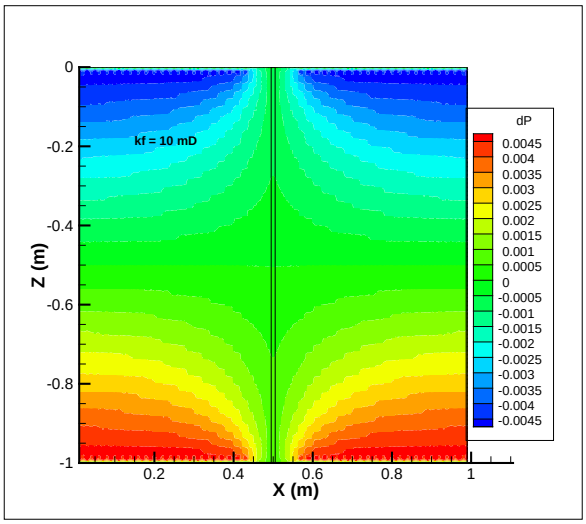

Figure 1: Pressure perturbation (in bars) for a model with one full-length fracture with $\kappa = 10^{-14}$ m^2.

We define the Flow Ratio (R) to be the ratio of the mass flow across a fractured model domain to that in the same domain with no fractures. The behaviour of R for the present example as a function of the number of fractures is shown in Figure 2. With even a single fracture the flow ratio is ~300. The flow through the model domain is thus completely dominated by the presence of just a single fracture. Due to the linearity of the model this conclusion will apply to any other system at any length scale with a similar proportion (1%) of fracture volume, fracture distribution and ratio of fracture to matrix permeability. It is expected that the flow will remain fracture-dominated except in the limits where the fracture permeabilities become comparable to those of the matrix or the relative fracture spacing becomes much larger than in this example.

Excepting the slightly off-trend result for the model with three fractures shown in Figure 2, the trend of flow ratio with number of fractures is close to linear. It was not possible to extend the calculation beyond four fractures as the requirement that fractures be fully resolved results in extremely large models which are impractical to run at present.

Extrapolating the linear trend in figure 2 gives a flow ratio of ~31,000 for 100 fractures, i.e., when the model domain is comprised completely of fracture material. This is ~20% higher than the expected result of 25,000, derived from Darcy's Law but using the fracture permeability instead of that for the matrix. Evidently there is some deviation from the linear trend as the number of fractures becomes large or there is some inaccuracy in the results for small numbers of fractures.

3.4.2 Parallel interior fractures

A more interesting situation occurs when there are one or more fractures which are completely internal to the rock matrix and aligned with the direction of flow. These fractures do not provide a connected path across the model domain so it is not obvious how they will affect the total flow across the sample.

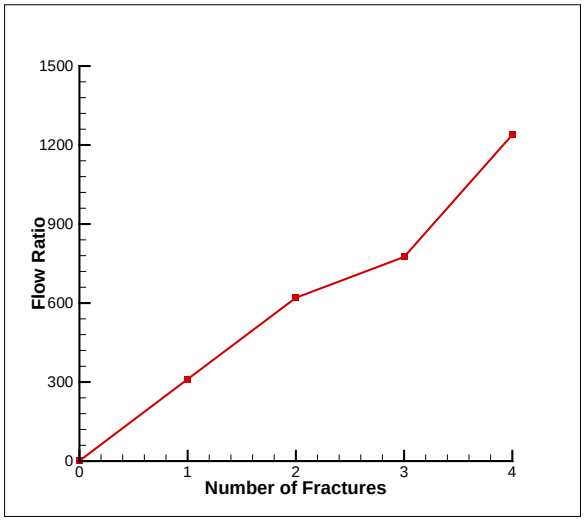

Figure 2: Flow ratio for a model with multiple full-length fractures parallel to the direction of flow.

We now show results for a particular model where the fractures have length of 0.4 m and a width of 0.01 m. Permeabilities and other rock properties, and the model setup are the same as those described in section 3.4.1.

Figure 3 shows a typical pattern for the pressure perturbation created by the fractures within the block. The pressure perturbation appears to be the same in every fracture – a pressure drop at the upstream tip of each fracture and an equal and opposite enhancement at the downstream end. A consequence of these opposing pressure changes is that the pressure drop along each fracture is very small. This is a result of the fracture permeability being large compared to the surrounding matrix and the fact that the pressure must be continuous across the fracture-matrix boundary.

Figure 4 shows the flow ratio R for this model as a function of the number of fractures (or equivalently, the fracture density). It turns out that there is a simple theoretical limit for R as the number of fractures increases. This is derived by requiring that the steady-state flow across the model domain must be the same for matrix and fracture in this limit. The general expression for R is:

$$R = k_f/k_m \,/\, [\, F/L + k_f/k_m(1 - F/L)\,], \qquad (1)$$

where L is the width of the model domain (1 m here), F the fracture length (0.4 m), and k_m and k_f are the matrix and fracture permeabilities. R then depends only on two ratios: the matrix to fracture permeability and the domain width to the length of the fractures.

For the case where the fracture permeability is much greater than that in the matrix R takes a particularly simple form:

$$R = 1/(1- F/L). \qquad (2)$$

This limit is shown by the blue dashed line in the figure, which shows that even with 10 fractures the calculated value of R is already approaching the theoretical limit of 1/(1-0.4) = 1.667.

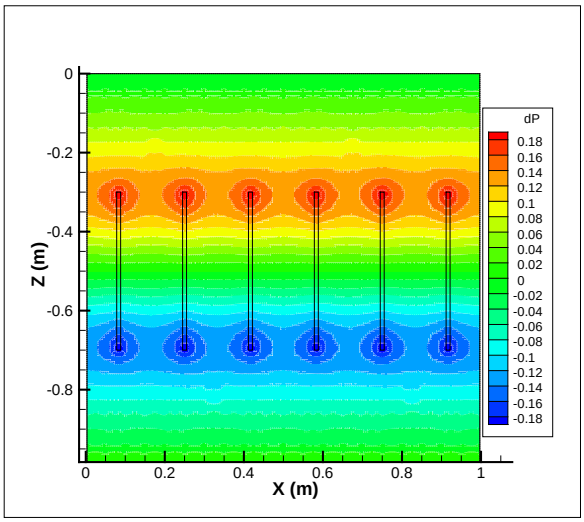

Figure 3: Pressure perturbation (in bars) for a system of six internal fractures. Note that the same pressure drop occurs over each fracture.

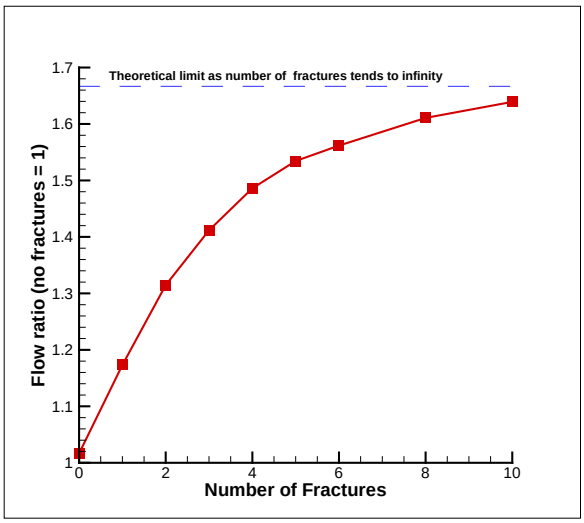

Figure 4: Flow ratio as a function of the number of fractures.

Equation (2) is obviously not valid when the fracture length F is equal to L, i.e. for full length fractures, and in this case the general equation (1) should be used.

It is noteworthy that the theoretical limit for R in equation (1) predicts only modest permeability enhancements in the presence of internal fractures which are short compared to the length scale the model. In the present case the largest enhancement is 1.667 times. This is in contrast to the

example of a full length fracture given in 3.4.1 where R ~300 for a single fracture.

3.4.3 Fracture Orientation

Thus far, we have considered only fractures which are aligned with the prescribed direction of flow in the model. This will in general not be the case and so in this section we derive the flow ratio for a single fracture as a function of its orientation with respect to this flow direction. In the model the fracture is 0.5 m long and 0.01 m wide, with a permeability of 1 Darcy. The initial and boundary conditions are identical to those used previously.

Figure 5 shows the pressure perturbation when the fracture is rotated at 50° with respect to the flow direction. As with the example in figure 3, the fracture induces a pressure deficit at its upstream tip and an enhancement of similar magnitude at the downstream tip. In this case the amplitude of the pressure perturbation is modulated in a non-trivial way – the resulting flow ratio R is shown in Figure 6. This shows the effect of the fracture is smallest when it lies across the flow direction, and largest when it is aligned with that direction. At small angles R differs by only a few percent from unity and at large angles R reaches ~1.3 – i.e. the fracture has a comparatively modest effect on the bulk permeability of the rock sample.

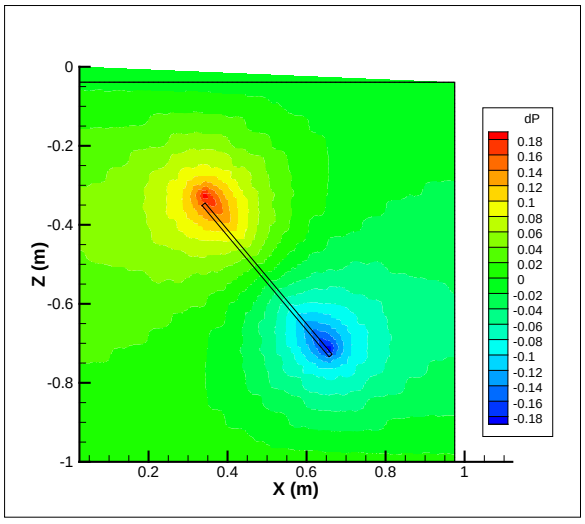

Figure 5: Pressure perturbation (in bars) for a single internal fracture rotated at 50° to the direction of flow.

3.4.4 Random fracture network

Finally, we present an example of flow across a random fracture network. This has been generated by defining the centres and orientations of ten fractures randomly from a uniform probability distribution. Figure 7 shows the steady-state pressure perturbation for this model. The main perturbations are concentrated in two locations – the negative (blue) ones near the most 'upstream' fracture tips (reminiscent of figure 3) while the major positive perturbations are further downstream and near the domain boundaries. The flow ratio for this model is 1.844. This is a quite modest enhancement in the bulk permeability of the sample, and is due to the fracture network not being fully-connected in the direction of flow, i.e. from the lower to upper boundary.

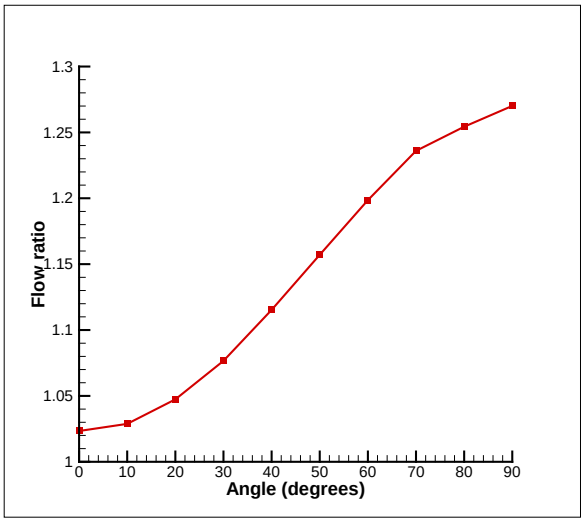

Figure 6: Flow ratio for a single internal fracture rotated through the indicated angle with respect to the direction of flow.

The behaviour of this fracture network is complicated, and it seems likely that there will be much variation in the flow ratio/bulk permeability depending on the distribution and connectedness of the fractures. Characterising networks like this is a statistical problem and to draw any general conclusions will require a far larger sample of random networks.

One future aim of this project is to develop techniques to simulate a sufficient number of fracture networks in this way with probability distributions for fracture width, spacing, and orientation specified by observation of a TVZ geothermal field (e.g Massiot et al., 2015).

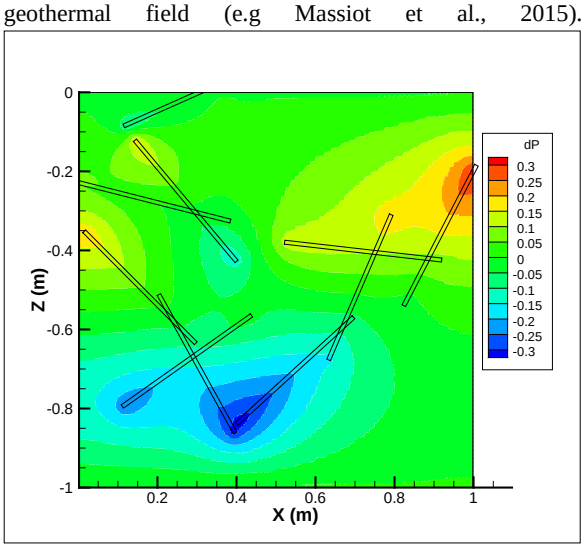

Figure 7: Pressure perturbation (bars) for a model with ten randomly-placed, randomly-orientated fractures.

4. ROCK MECHANICS

The fluid-flow models in the previous section can be combined with mechanical finite-element models to investigate the interaction of fluid pressure and flow around cracks with stresses in the host rock. A 2-dimensional finite-element model (Buiter and Ellis, 2012; Ellis et al., 2011) was used to model brittle and tensile deformation for a vertical cross-section with the same dimensions as the models in section 3. Rock properties were loosely based on measured values for andesite (Siratovich et al., 2012; 2014). We used a cohesive frictional strength of 25 MPa, a tensile strength of 15 MPa and matrix permeability of 10^{-17} m^2. Lower-strength fractures had a low frictional cohesion of 1 MPa so that cracks acted as low-strength inclusions, with a matrix permeability of 10^{-12} m^2. The same fluid pressure boundary conditions were applied as in the previous section. In addition, the 1×1m model domain was pulled apart from the left and right-hand-sides at a constant extensional strain-rate of 2×10^{-13} s^{-1} to induce tensional failure. Once tensile yield was exceeded, an algorithm in the code replaced intact rock with a much lower-strength material simulating fracture propagation (e.g., Misra et al., 2015). Tensile opening was modelled by computing the dynamic pressure at each step and using it to determine whether the tensile yield limit has been exceeded. Where this yield condition is met, and an element is adjacent to an already "open" element (e.g., the imposed crack), material is overwritten by low-strength material simulating the weakening effects of fracture formation. The adjacency criterion ensures that tensile fractures do not open spontaneously, but rather require propagation from an existing flaw.

The normalized maximum tensile stress at the tips of a fracture depends on the orientation of the fracture with respect to axial stress (Misra et al., 2009). For a constant fracture length, the tensile stress attains its maximum value for α = 45°, and this influences the relative importance of shear-band formation vs. tensile wing fractures growing from the fracture tips. Our numerical experiment of fluid flow-fracture interaction demonstrates the effect that misoriented fractures have on the stress field and fracture opening by comparing a fracture initially at 45° to the extension direction with a fracture that is normal to the extension direction (figure 8).

Figures 8 and 9 show how both fractures propagate with time as tensile strength is locally exceeded at the fracture tips. The fracture propagation from the initially-misoriented fracture dominates; this is because the tensile stresses increase with length of the fracture, and the misoriented part of the fracture initially perturbs stress magnitudes and directions more that the fracture on the right which is perpendicular to extension direction. There is also an interaction with the boundary conditions for the left-hand fracture which accentuates its effect on stresses (i.e., the diagonal line of perturbed stresses emanating from the left-hand-lower corner). As the left-hand fracture lengthens, it comes to dominate the perturbation in fluid flow, a result that is consistent with the fluid-flow experiments in section 3. This demonstrates that the initial orientation of inherited fractures cf. the extension direction can determine to a large degree whether a fracture will propagate and significantly influence the permeability and fluid pressure around it.

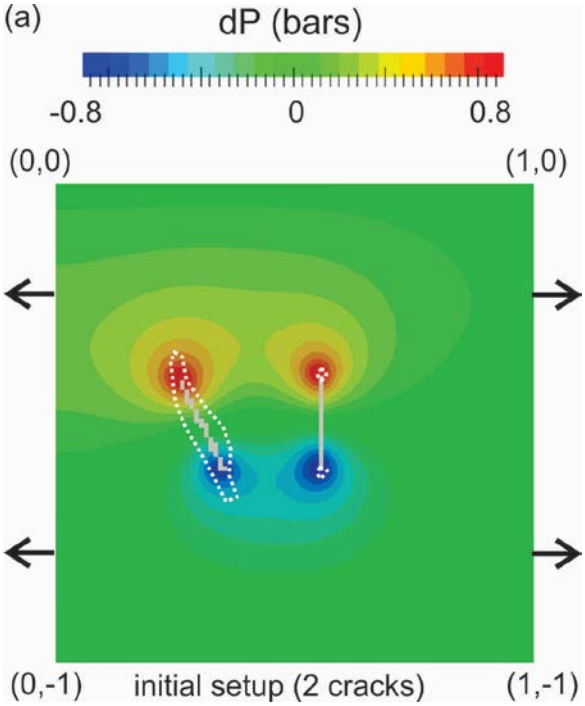

Figure 8: Pressure perturbation at the beginning of the fluid-mechanical experiment. Black arrows show extension direction imposed at left and right-hand-sides. White dashed contours show region where extensional stress direction is > 10° misoriented from horizontal, i.e. extent of stress perturbation around fractures.

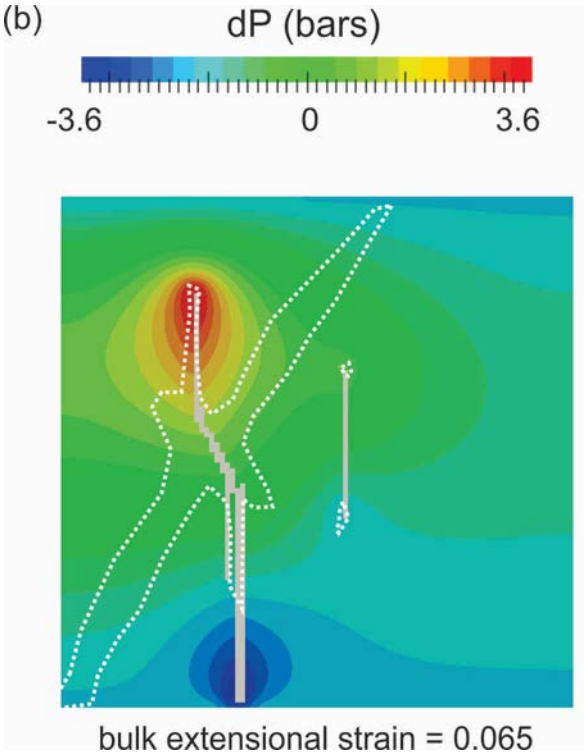

Figure 9: Pressure perturbation after 100 years extension. The left-hand fracture, initially misoriented to the extension direction, undergoes fracture propagation and interaction with a shear zone that nucleates at the left-lower corner of the model. As the left-hand fracture grows it completely dominates the system.

5. SUMMARY AND OUTLOOK

In this paper we have presented some early steps in a project which aims to understand how fractures (and their physical properties, distribution and orientation in space with respect to the local stress state) contribute to the bulk permeability of reservoir rocks, with particular emphasis on TVZ geothermal fields.

Some initial modelling of metre-scale rock samples containing simple fracture networks with idealised rectangular fractures has been carried out. For these models we use matrix permeabilties typical of lavas in the Rotokawa Andesite, and fracture permeabilities up to 1 Darcy. Fluid flow modelling of these fracture networks suggests that modifications to the bulk permeability are most a few 10's percent for disconnected fractures but can be very high, ~100x or more, for connected fractures. In the latter case the fracture permeability dominates the bulk permeability. These results will also apply at reservoir scales because the models are constructed to use essentially constant fluid properties and the resulting linear behaviour makes them independent of any length scale.

A rock-mechanical model of a disconnected two-fracture system is also presented. This shows pressure perturbations caused by the fractures of similar character to the fluid flow modelling but, in addition, shows the effect of an applied stress on a fracture which is not aligned with that stress. These preliminary mechanical experiments demonstrate the ongoing interaction between a propagating crack and the fluid pressure perturbation around it. We have not investigated the scaling relationships (i.e., the relative stress perturbation for different initial crack lengths, orientations, and fluid pressures) in these models yet.

In the future, both fluid flow and rock-mechanical modelling techniques will be applied to more complex fracture systems and with more realistic fracture geometries, again with the aim of understanding how the effective bulk permeabilities might behave at larger length scales, and under different states of stress. In these studies, we plan to use realisations of fracture networks generated from statistical models of fracture networks from particular New Zealand geothermal fields (e.g. Massiot et al., 2015).

Further effort will also include combining the fluid and mechanical modelling codes into a single thermo-hydro-mechanical (THM) code so that the coupled effects of fluid pressures, temperatures and stresses can be properly treated. This will allow, for example, studies of near-well (fracture dominated) permeabilities when cool fluid is injected into a high temperature geothermal reservoir.

ACKNOWLEDGEMENTS

The authors gratefully acknowledge funding for this work from GNS's Geothermal Supermodels programme and the Sarah Beanland Memorial Scholarship awarded by GNS Science for funding C. Massiot's PhD thesis.

REFERENCES

Barton, C. A., D. Moos, L. Hartley, S. Baxter, L. Foulquier, H. Holl, R. Hogarth (2013), Geomechanically coupled simulation of flow in fractured reservoirs, Proceedings, Thirty-Eighth Workshop on Geothermal Reservoir Engineering.

Baghbanan, A. and Jing, L. (2008), Stress effects on permeability in a fractured rock mass with correlated fracture length and aperture, International Journal of Rock Mechanics and Mining Sciences, 45, 1320-1334, doi: 10.1016/j.ijrmms.2008.01.015

Brace, W. F. (1980), Permeability of crystalline and argillaceous rocks, International Journal of Rock Mechanics and Mining Sciences & Geomechanics Abstracts, 17, 241–251, doi:10.1016/0148-9062(80)90807-4.

Buiter, S., Ellis, S.: (2012). SULEC: Benchmarking a new ALE finite- element code. Geophysical Research Abstracts, EGU General Assembly 14: EGU2012-7528.

Davatzes, N. C. and S. H. Hickman (2010a), Stress, fracture, and fluid-flow analysis using acoustic and electrical image logs in hot fractured granites of the Coso Geothermal Field, California, U.S.A., in

Dipmeter and borehole image log technology, edited by M. Pöppelreiter, C. García-Carballido and M. Kraaijveld, AAPG Memoir, 92, 259-293, doi:10.1306/13181288M923134.

Davatzes, N. C. and S.H. Hickman (2010b), The feedback between stress, faulting, and fluid flow: Lessons from the Coso Geothermal Field, CA, U.S.A., Proceedings, World Geothermal Congress 2010.

Doe, T., McLaren, R., Dershowitz, W .: Discrete Fracture Network Simulations of Enhanced Geothermal Systems., Proceedings, Thirty-Ninth Workshop on Geothermal Reservoir Engineering, Stanford, 2014.

Ellis, S.M., T.A. Little, L.M., Wallace, B.R. Hacker, and S.J.H. Buiter (2011), Feedback between rifting and diapirism can exhume ultrahigh-pressure rocks, Earth & Planet. Sci. Lett. 311, 427-438, doi: doi:10.1016/j.epsl.2011.09.031.

Haukwa, C.B.: AMESH, A mesh creating program for the Integral Finite Difference Method, User Manual. Lawrence Berkeley Laboratory Report. (1998).

Huang, H, Plummer, M, Podgorney, R., Simulated evolution of fractures and fracture networks subject to thermal cooling: A coupled discret element and heat conduction model., Proceedings, Thirty-Eigth Workshop on Geothermal Reservoir Engineering, Stanford, 2013.

Ito, T. and M. D. Zoback (2000), Fracture permeability and in situ stress to 7 km depth in the KTB scientific drillhole, Geophysical Research Letters, 27, 1045–1048, doi:10.1029/1999GL011068.

Kissling, W.M.: A testbed for a new-generation geothermal simulator. Proc. 36th New Zealand Geothermal Workshop, Auckland, New Zealand. (2014).

Laubach, S. E., J. E. Olson and J. F. W. Gale (2004), Are open fractures necessarily aligned with maximum horizontal stress?, Earth and Planetary Science Letters, 222, 191–195, doi:10.1016/j.epsl.2004.02.019.

Litchfield, N. J., R. Van Dissen, R. Sutherland, P. M. Barnes, S. C. Cox, R. Norris, R. J. Beavan, R. Langridge, P. Villamor, K. Berryman, M. Stirling, A. Nicol, S. Nodder, G. Lamarche, D. J. A. Barrell, J. R. Pettinga, T. Little, N. Pondard, J. J. Mountjoy and K. Clark (2014), A model of active faulting in New Zealand, New Zealand Journal of Geology and Geophysics, 57, 32-56, doi:10.1080/00288306.2013.854256

Maffucci, R., Bigi, S., Corrado, S., Chiodi, a., Di Paolo, L., Giordano, G., & Invernizzi, C. (2015). Quality assessment of reservoirs by means of outcrop data and “discrete fracture network” models: The case history of Rosario de La Frontera (NW Argentina) geothermal system. Tectonophysics, 647-648, 112–131. doi:10.1016/j.tecto.2015.02.016

Massiot, C., McNamara, D.D., Nicol, A. and John Townend (2015), Fracture Width and Spacing Distributions from Borehole Televiewer Logs and Cores in the Rotokawa Geothermal Field, New Zealand, World Geothermal Congress 2015

McLean, K. and D. D. McNamara (2011), Fractures Interpreted from Acoustic Formation Imaging Technology: Correlation to Permeability, Proceedings, Thirty-Sixth Workshop on Geothermal Reservoir Engineering.

McNamara, D.D., Sewell, S., Buscarlet, E. and I.C. Wallis (2015), A review of the Rotokawa Geothermal Field, New Zealand, Geothermics, doi: 10.1016/j.geothermics.2015.07.007

McNamara, D.D., Massiot, C., Lewis, B. and I.C. Wallis (2014), Heterogeneity of structure and stress in the Rotokawa Geothermal Field, New Zealand, Journal of Geophysical Research: Solid Earth, 120, 1243-1262, doi: 10.1002/2014JB011480

Milicich, S.D., Clark, J.P.,. Wong, C. and M. Askari (2015), A review of the Kawerau Geothermal Field, New Zealand, Geothermics, doi: 10.1016/j.geothermics.2015.06.012

Milicich, S.D., Wilson, C.J.N., Biganll, G., Pezaro, B. and C. Bardsley (2013), Reconstructing the geological and structural history of an active geothermal field: A case study from New Zealand, Journal of Volcanology and Geothermal Research, 262, 7-24, doi: 10.1016/j.jvolgeores.2013.06.004

Misra, S., N. Mandal, R. Dhar and C. Chakraborty (2009), Mechanisms of deformation localization at the tips of shear fractures: Findings from analogue experiments and field evidence. J. Geophys. Res. Solid Earth. DOI: 10.1029/2008JB005737.

Misra, S., S. Ellis, and N. Mandal (2015), Fault damage zones in mechanically layered rocks: The effects of planar anisotropy, J. Geophys. Res. Solid Earth, 120, doi:10.1002/2014JB011780.

Nicol, A., J. Walsh, K. Berryman and P. Villamor (2006), Interdependence of fault displacement rates and paleoearthquakes in an active rift, Geology, 34, 865 doi:10.1130/G22335.1.

Philipp, S. L., F. Afşar and A. Gusmundsson (2013), Effects of mechanical layering on hydrofracture emplacement and fluid transport in reservoirs, Frontiers in Earth Science, 1, 1-19, doi:10.3389/feart.2013.00004

Pruess, K.: TOUGH2, A general purpose Numerical Simulator for multiphase fluid and heat flow. Lawrence Berkeley Laboratory Report, LBL-29400 (1990).

Sausse, J., M. Fourar and A. Genter (2006), Permeability and alteration within the Soultz granite inferred from geophysical and flow log analysis, Geothermics, 35, 544–560, doi:10.1016/j.geothermics.2006.07.003.

Sherburn, A., Sewell, S.M., Bourguignon, S., Cumming, W., Bannister, S., Bardsley, C., Winick, J., Quinao, J. and I.C. Wallis (2015), Microseismicity at Rotokawa Geothermal Field, New Zealand, 2008-2012, Geothermics, 54, 23-34, doi: 10.1016/j.geothermics.2014.11.001

Sheridan, J. M. and S. H. Hickman (2004), In situ stress, fracture, and fluid flow analysis in Well 38C-9: an enhanced geothermal system in the Coso geothermal field. Proceedings, Twenty-Ninth Workshop on Geothermal Reservoir Engineering.

Siratovich, P. A., Davidson, J.,Villeneuve, M., Gravley, D., Kennedy, B., Cole, J., Wyering, L., and Price, L.: Physical and mechanical properties of the Rotokawa Andesite from production wells RK 27_L2, RK 28 and RK 30. Proc. 34th New Zealand Geothermal Workshop, Auckland, New Zealand. (2012).

Siratovich, P.A. and 4 others.: Physical property relationships of the Rotokawa Andesite, a significant geothermal reservoir in the Taupo Vaolcanic Zone, New Zealand. Geothermal Energy, 2/10, (2014).

Wagner, W. and 14 others.: The IAPWS Industrial Formulation 1997 for the thermodynamic properties of water and steam. Transactions of the ASME, 150, pp 150-182 (2000).

Wallis, I. C., D. D. McNamara, J. Rowland and C. Massiot (2012), The nature of fracture permeability in the basement greywacke at Kawerau Geothermal Field, New Zealand, Proceedings, Thirty-seventh Workshop on Geothermal Reservoir Engineering.

Wallis, I. C., C. J. Bardsley, T. S. Powell, J. V. Rowland and J. M. O'Brien (2013), A structural model for the Rotokawa Geothermal Field, New Zealand, 35th New Zealand Geothermal Workshop: 2013 Proceedings.

Wilson, C.J.N. and J. V. Rowland (2015), The volcanic, magmatic and tectonic setting of the Taupo Volcanic Zone, New Zealand, reviewed from a geothermal perspective, Geothermics, doi: 10.1016/j.geothermics.2015.06.013

Wood, C. P., R. L. Brathwaite and M. D. Rosenberg (2001), Basement structure, lithology and permeability at Kawerau and Ohaaki geothermal fields, New Zealand, Geothermics, 30, 461-481, doi:10.1016/S0375-6505(01)00003-7.